REPORT 1213

MINIMUM-DRAG DUCTED AND POINTED BODIES OF REVOLUTION BASED ON LINEARIZED SUPERSONIC THEORY [1]

By Hermon M. Parker

SUMMARY

The linearized drag integral for bodies of revolution at supersonic speeds is presented in a double-integral form which is not based on slender-body approximations but which reduces to the usual slender-body expression in the proper limit. With the aid of a suitably chosen auxiliary condition, the minimum-external-wave-drag problem is solved for a transition section connecting two semi-infinite cylinders. The projectile tip is a special case and is compared with the Von Kármán projectile tip. Calculations are presented which indicate that the method of analysis gives good first-order results in the moderate supersonic range.

INTRODUCTION

In making the slender-body approximation to the linearized supersonic-flow theory for bodies of revolution, a basic approximation leads to replacing the axial source distribution with the cross-sectional-area derivative. Slender-body theory, therefore, becomes linear in the superposition sense for cross-sectional areas as well as for sources or fields in contrast to linear supersonic-flow theory which is linear in the superposition sense for sources or fields but not for areas. Making the slender-body approximation, however, eliminates a large part of the Mach number dependence of the results. Lighthill (ref. 1) has shown that this basic approximation, for sufficiently smooth bodies, has the same mathematical order of accuracy as the linearized supersonic-flow equation. Ward (ref. 2) has extended the generality of slender-body theory by presenting a drag expression which is valid for a body with a finite slope at the base. Lighthill (ref. 3) has, at the price of a large increase in complexity, modified slender-body theory to include area-derivative discontinuities at a finite number of points.

In 1935 Von Kármán (ref. 4) determined the minimum-wave-drag projectile tip. Later Sears (ref. 5) and Haack (ref. 6) determined minimum-wave-drag shapes for projectile tips and closed bodies of revolution subject to various combinations of auxiliary conditions of constant length, constant caliber, and constant volume. The Von Kármán tip and the Sears-Haack bodies are based on slender-body theory. In contrast to the minimum-drag bodies of given volume, which are accepted as reasonably good first-order results, the minimum-drag projectile tips and open-nosed bodies which have been derived from slender-body theory are subject to more severe restrictions on the range and conditions for validity. Busemann (ref. 7) pointed out this fact for the Von Kármán projectile tip in 1941. In the late 1930's Ferrari made studies of the minimum-drag projectile tip and length-caliber body problems. Recently, Ferrari (refs. 8 and 9) has considered the length-caliber body and ducted-body minimum-drag problems on the basis of linear theory without resorting to slender-body approximations. He obtains source-distribution functions which involve elliptic integrals that have to be treated numerically.

This report presents the linearized-drag integral for bodies of revolution in a double-integral form which is not based on slender-body approximations but which reduces to Ward's drag expression in the proper limit. With the aid of a suitably chosen auxiliary condition, the minimum-external-wave-drag problem for a transition section connecting two semi-infinite cylinders is solved. The source distribution, the minimum-wave drag, the slopes at the ends of the section, and the radius at one intermediate point are obtained in terms of elementary functions. The entire shape is given in an integral form amenable to numerical evaluation.

SYMBOLS

C	constant factor in source-distribution function, ft/sec
C_D	drag coefficient
D	drag, lb
f	source-distribution function
f'	derivative of f with respect to its argument
M	free-stream Mach number
r	radius in cylindrical coordinates
R	general radius of point on body
R_1	radius of downstream cylinder
R_2	radius of upstream cylinder
$A'(x)$, $A''(x)$	first and second derivatives of cross-sectional area
U	free-stream velocity, ft/sec
v_r	radial velocity, ft/sec
v_x	axial velocity, ft/sec
x	axial distance in cylindrical coordinates
x_0	position of first disturbance on control surface

[1] Supersedes NACA TN 3189, 1954.

X	axial distance for general point on body
$\beta=\sqrt{M^2-1}$	
$\delta f'$	variation in derivative of source-distribution function
ρ	free-stream density, slugs/cu ft
λ	arbitrary constant
ξ,η	dummy variables of integration
ξ_0, η_0	position on axis where sources begin
ϕ	disturbance potential

All distances are made dimensionless by measuring them in the units of length of the transition section.

ANALYSIS

DRAG INTEGRAL

The linearized-flow equation for the case of axial symmetry is (ref. 4)

$$\frac{\partial^2\phi}{\partial r^2}+\frac{1}{r}\frac{\partial\phi}{\partial r}-\beta^2\frac{\partial^2\phi}{\partial x^2}=0 \tag{1}$$

where ϕ is the disturbance potential, $\beta^2=M^2-1$, and M is the free-stream Mach number. The general solution of equation (1) is (ref. 10)

$$\phi(x,r)=\int_{\infty}^{0}f(x-\beta r\cosh u)du=-\int_{-\infty}^{x-\beta r}\frac{f(\xi)d\xi}{\sqrt{(x-\xi)^2-\beta^2r^2}} \tag{2}$$

The corresponding disturbance velocities are

$$\frac{\partial\phi}{\partial x}=v_x(x,r)=\int_{\infty}^{0}f'(x-\beta r\cosh u)du=-\int_{-\infty}^{x-\beta r}\frac{f'(\xi)d\xi}{\sqrt{(x-\xi)^2-\beta^2r^2}} \tag{3}$$

and

$$\frac{\partial\phi}{\partial r}=v_r(x,r)=-\int_{\infty}^{0}f'(x-\beta r\cosh u)\beta\cosh u\,du$$
$$=\frac{1}{r}\int_{-\infty}^{x-\beta r}\frac{f'(\xi)(x-\xi)d\xi}{\sqrt{(x-\xi)^2-\beta^2r^2}} \tag{4}$$

The general solution is interpreted physically as the disturbance potential of a distribution of axial sources. The source-distribution function $f(\xi)$ is fixed by satisfying the boundary condition that the body surface be a stream surface.

Applying the momentum and continuity theorems to the fluid within a cylindrical surface of radius R_1 and with the symmetry axis parallel to the stream (hereinafter referred to as the control surface) and using the fact that free-stream conditions prevail at the two ends of the cylinder, $x=\infty$ and $x=-\infty$, yield the usual expression for the drag (ref. 4)

$$D=-2\pi\int_{-\infty}^{\infty}\rho R_1v_x(x,R_1)v_r(x,R_1)\,dx \tag{5}$$

If a position $x=L$ on the control surface is chosen so that, for $x\geqq L$, either v_r or v_x vanishes on the control surface, and if x_0 is the position of the first disturbance on the control surface, equation (5) reduces to

$$D=-2\pi\int_{x_0}^{L}\rho R_1v_x(x,R_1)\,v_r(x,R_1)\,dx \tag{6}$$

Substituting expressions (3) and (4) for the velocities into equation (6), where $\xi_0=\eta_0=x_0-\beta R_1$, the position on the axis where the sources begin, yields

$$D=2\pi\rho\int_{x_0}^{L}\left[\int_{\xi_0}^{x-\beta R_1}\frac{f'(\xi)(x-\xi)d\xi}{\sqrt{(x-\xi)^2-\beta^2R_1^2}}\right]\left[\int_{\eta_0}^{x-\beta R_1}\frac{f'(\eta)d\eta}{\sqrt{(x-\eta)^2-\beta^2R_1^2}}\right]dx \tag{7}$$

or

$$D=2\pi\rho\int_{x_0}^{L}\left[\int_{\xi_0}^{x-\beta R_1}\int_{\eta_0}^{x-\beta R_1}\frac{f'(\xi)f'(\eta)(x-\xi)\,d\xi\,d\eta}{\sqrt{(x-\xi)^2-\beta^2R_1^2}\sqrt{(x-\eta)^2-\beta^2R_1^2}}\right]dx \tag{8}$$

The basic slender-body approximation reduces the integral over ξ in equation (7) to f(x). The use of equation (4) for small values of r and the boundary condition $\frac{dr}{dx}=\frac{v_r}{U}$ gives $f(x)$ proportional to the axial derivative of the cross-sectional area. The slender-body approximation thus reduces the integral of equation (8) to a double integral (over x and η). In principle, the integral in equation (8) may be reduced to a double integral over ξ and η by interchanging the order of integration and performing the integration over x. When this process is attempted in equation (8), however, the integration over x involves elliptic integrals and no essential advantage is gained.

However, the drag integral may be reduced to a double integral in the following manner. Equation (8) is rewritten with the dummy variables ξ and η interchanged. Addition of the interchanged and original expressions and division by 2 yield

$$D=\pi\rho\int_{x_0}^{L}dx\int_{\xi_0}^{x-\beta R_1}\int_{\eta_0}^{x-\beta R_1}\frac{f'(\xi)f'(\eta)(x-\xi+x-\eta)d\xi\,d\eta}{\sqrt{(x-\xi)^2-\beta^2R_1^2}\sqrt{(x-\eta)^2-\beta^2R_1^2}} \tag{9}$$

Interchanging the order of integration yields

$$D=\pi\rho\int_{\xi_0}^{L-\beta R_1}\int_{\eta_0}^{L-\beta R_1}f'(\xi)f'(\eta)d\xi\,d\eta\int_{\substack{\xi+\beta R_1\\ \eta+\beta R_1}}^{L}\frac{(x-\xi+x-\eta)dx}{\sqrt{(x-\xi)^2-\beta^2R_1^2}\sqrt{(x-\eta)^2-\beta^2R_1^2}} \tag{10}$$

where the lower limit of the integral over x is $\xi+\beta R_1$ or $\eta+\beta R_1$, whichever is the larger. The results of the integration over x is (see the appendix for the details of the integration)

$$\int_{\substack{\xi+\beta R_1\\ \eta+\beta R_1}}^{L}\frac{(x-\xi+x-\eta)dx}{\sqrt{(x-\xi)^2-\beta^2R_1^2}\sqrt{(x-\eta)^2-\beta R_1^2}}=\left[\cosh^{-1}\left|\frac{(x-\xi)(x-\eta)-\beta^2R_1^2}{\beta R_1(\xi-\eta)}\right|\right]_{\substack{\xi+\beta R_1\\ \eta+\beta R_1}}^{L}=\cosh^{-1}\left|\frac{(L-\xi)(L-\eta)-\beta^2R_1^2}{\beta R_1(\xi-\eta)}\right| \tag{11}$$

and the drag becomes

$$D=\pi\rho\int_{\xi_0}^{L-\beta R_1}\int_{\eta_0}^{L-\beta R_1}f'(\xi)f'(\eta)\cosh^{-1}\left|\frac{(L-\xi)(L-\eta)-\beta^2R_1^2}{\beta R_1(\xi-\eta)}\right|d\xi\,d\eta \tag{12}$$

Equation (12) gives the drag of an axial distribution of sources $f(\xi)$ which begins at ξ_0 and is subject to the condition that there is no momentum flow through the control cylinder of radius R_1 for $x \geqq L$.

In the slender-body approximation, equation (12) reduces to Ward's drag expression as follows. Use of the expression for the radial velocity (eq. (4)) for small values of r and the boundary condition $\frac{dr}{dx}=\frac{v_r}{U}$ give

$$f(x)=\frac{U}{2\pi}A'(x) \tag{13}$$

where $A'(x)$ is the axial derivative of the cross-sectional area. For small values of R_1, βR_1 may be neglected in the limits of the integrals in equation (12) and the $\cosh^{-1}$ factor may be approximated by

$$\cosh^{-1}\left|\frac{(L-\xi)(L-\eta)-\beta^2R_1^2}{\beta R_1(\xi-\eta)}\right|=\log\left[(L-\xi)(L-\eta)\right]-\log|\xi-\eta|-\log\frac{\beta R_1}{2} \tag{14}$$

Simple manipulation, based on the assumption that $A'(\xi)$ is continuous and $A'(\xi_0)=0$, gives the Ward drag formula

$$D=-\frac{\rho U^2}{4\pi}\int_{\xi_0}^{L}\int_{\eta_0}^{L}A''(\xi)A''(\eta)\log|\xi-\eta|\,d\xi d\eta+\frac{\rho U^2}{2\pi}A'(L)\int_{\xi_0}^{L}A''(\xi)\log(L-\xi)d\xi-\frac{\rho U^2}{4\pi}[A'(L)]^2\log\frac{\beta R_1}{2} \tag{15}$$

MINIMUM-DRAG PROBLEM

The problem of determining the shape of a transition section connecting two semi-infinite cylinders for minimum external wave drag may be formulated in the following way. (See fig. 1.) The upstream and downstream semi-infinite cylinders are of radius R_2 and R_1, respectively. The length of the transition section is taken as the unit in which all distances are measured. The cylinder of radius R_1 is chosen as the control surface.

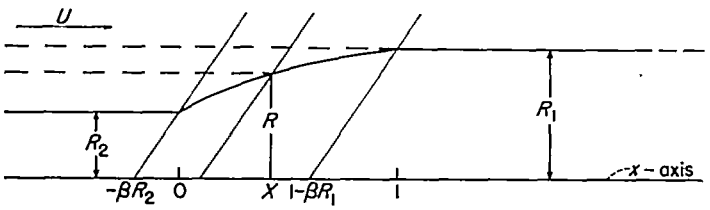

FIGURE 1.—Configuration treated.

Figure 1 is drawn for the case $R_2<R_1$. However, the statement of the problem is the same as for $R_2>R_1$ since only the appropriate changes in sign occur. Equation (12) for the drag becomes

$$D=\pi\rho\int_{-\beta R_2}^{1-\beta R_1}\int_{-\beta R_2}^{1-\beta R_1}f'(\xi)f'(\eta)\cosh^{-1}\left|\frac{(1-\xi)(1-\eta)-\beta^2R_1^2}{\beta R_1(\xi-\eta)}\right|d\xi d\eta \tag{16}$$

The auxiliary condition for the minimum-wave-drag problem is the requirement that the points $x=1$, $r=R_1$ and $x=0$, $r=R_2$ be on the same stream surface. In terms of mass flow this condition requires that the free-stream mass flow between the control cylinder of radius R_1 and the upstream cylinder of radius R_2 equals the mass flow out of the control cylinder between $x=\beta(R_1-R_2)$ and $x=1$; that is,

$$\rho U\pi(R_1^2-R_2^2)=\int_{\beta(R_1-R_2)}^{1}2\pi\rho R_1v_r(x,R_1)dx=\text{Constant} \tag{17}$$

or

$$\int_{\beta(R_1-R_2)}^{1}\int_{-\beta R_2}^{x-\beta R_1}\frac{f'(\xi)(x-\xi)d\xi}{\sqrt{(x-\xi)^2-\beta^2R_1^2}}dx=\frac{U}{2}(R_1^2-R_2^2)=\text{Constant} \tag{18}$$

Equation (18) is a particularly convenient form of the auxiliary condition in that the source-distribution function is the only unknown involved. A direct integration of the usual boundary condition would lead to an auxiliary condition involving, in addition, the unknown shape of the section. Without further approximations, the minimum-drag problem would be unmanageable. It appears impossible to obtain an auxiliary condition of constant volume involving the source-distribution function as the only unknown.

Interchanging the order of integration in the left member of equation (18) and integrating over x yield

$$\int_{-\beta R_2}^{1-\beta R_1}f'(\xi)\sqrt{(1-\xi)^2-\beta^2R_1^2}\,d\xi=\frac{U}{2}(R_1^2-R_2^2)=\text{Constant} \tag{19}$$

The problem of minimizing the drag given by equation (16), subject to the auxiliary condition given by equation (19), can be expressed in the usual manner of the calculus of variations. The expression

$$G(f', R_1, R_2)=\int_{-\beta R_2}^{1-\beta R_1}\int_{-\beta R_2}^{1-\beta R_1} f'(\xi)f'(\eta)\cosh^{-1}\left|\frac{(1-\xi)(1-\eta)-\beta^2R_1^2}{\beta R_1(\xi-\eta)}\right| d\xi d\eta+2\lambda\int_{-\beta R_2}^{1-\beta R_1} f'(\xi)\sqrt{(1-\xi)^2-\beta^2R_1^2}\,d\xi \tag{20}$$

(where constant factors have been absorbed into the arbitrary constant λ) must have a zero variation corresponding to an arbitrary small variation $\delta f'$ in f'; that is,

$$G(f'+\delta f', R_1, R_2)-G(f', R_1, R_2)=0$$

Combining two terms, after interchanging dummy variables and neglecting the term involving $(\delta f')^2$, yields

$$\int_{-\beta R_2}^{1-\beta R_1}\delta f'(\xi)\left[\int_{-\beta R_2}^{1-\beta R_1} f'(\eta)\cosh^{-1}\left|\frac{(1-\xi)(1-\eta)-\beta^2R_1^2}{\beta R_1(\xi-\eta)}\right| d\eta+\lambda\sqrt{(1-\xi)^2-\beta^2R_1^2}\right] d\xi=0 \tag{21}$$

Since the variation $\delta f'$ is arbitrary,

$$\int_{-\beta R_2}^{1-\beta R_1} f'(\eta)\cosh^{-1}\left|\frac{(1-\xi)(1-\eta)-\beta^2R_1^2}{\beta R_1(\xi-\eta)}\right| d\eta+\lambda\sqrt{(1-\xi)^2-\beta^2R_1^2}=0 \tag{22}$$

An integration by parts, with $f(-\beta R_2)=0$, yields

$$\int_{-\beta R_2}^{1-\beta R_1}\frac{f(\eta)\,d\eta}{(\xi-\eta)\sqrt{(1-\eta)^2-\beta^2R_1^2}}=\lambda=\text{Constant} \tag{23}$$

The integral equation (23) is the same equation that appears in the minimum-induced-drag problem in lifting-line airfoil theory.

The solution of the integral equation

$$\int_a^b\frac{F(y)\,dy}{\xi-y}=\text{Constant}$$

is

$$F(y)=\frac{Cy+C_1}{\sqrt{(b-y)(y-a)}}$$

Therefore, the solution of equation (23) is

$$f(\eta)=(C\eta-C_1)\sqrt{\frac{1+\beta R_1-\eta}{\eta+\beta R_2}} \tag{24}$$

The condition that $f(-\beta R_2)=0$ requires that $C_1=C\beta R_2$ therefore,

$$f(\eta)=C\sqrt{(\eta+\beta R_2)(1+\beta R_1-\eta)} \tag{25}$$

The source-distribution function for minimum wave drag is part of an ellipse. The constant C is fixed by satisfying the auxiliary condition, equation (19). The final result for the source-distribution function for minimum wave drag is

$$f(\eta)=\frac{4U(R_1^2-R_2^2)}{\pi(1-\beta R_1+\beta R_2)(1+3\beta R_1+\beta R_2)}\sqrt{(\eta+\beta R_2)(1+\beta R_1-\eta)} \tag{26}$$

Figure 2, which has an arbitrary vertical scale, shows the source distribution corresponding to the transition section of minimum wave drag.

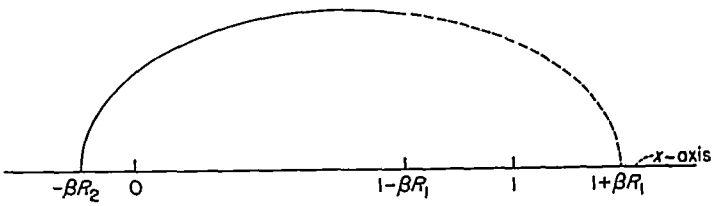

FIGURE 2.—Source distribution (arbitrary vertical scale) corresponding to transition section of minimum drag. Ellipse of which the distribution is a part is shown by dashed curve.

MINIMUM-DRAG SHAPE

The expression for the minimum-drag shape is analogous to the auxiliary condition given by equation (17) except that a control surface of arbitrary radius R is used, where R is the radius of the section at $x=X$ (see fig. 1); the shape is given by

$$\rho U\pi(R^2-R_2^2)=\int_{\beta(R-R_2)}^{X}2\pi\rho R v_r(x, R)\,dx$$

$$=2\pi\rho\int_{\beta(R-R_2)}^{X}\left[\int_{-\beta R_2}^{X-\beta R}\frac{f'(\xi)(x-\xi)\,d\xi}{\sqrt{(x-\xi)^2-\beta^2R^2}}\right]dx \tag{27}$$

Interchanging the order of integration, integrating over x, and substituting the source-distribution function yield

$$\beta^2(R^2-R_2^2)=\frac{8\beta^2(R_1^2-R_2^2)}{\pi(1-\beta R_1+\beta R_2)(1+3\beta R_1+\beta R_2)}\int_{-\beta R_2}^{X-\beta R}\frac{\left(\frac{1+\beta R_1-\beta R_2}{2}-\xi\right)\sqrt{(X-\xi)^2-\beta^2R^2}}{\sqrt{(\xi+\beta R_2)(1+\beta R_1-\xi)}}\,d\xi \tag{28}$$

Since all the radii in equation (28) are multiplied by β, one calculation gives a family of shapes for which, at a given value of X, $\beta R(X)=\text{Constant}$. Thus the minimum-drag shape obeys the Göthert similarity rule (ref. 11).

At the general point (X, R), the integral in equation (28) involves elliptic integrals and cannot be evaluated in elementary form. However, at one particular value of X, corresponding to the center of the source-distribution ellipse, the integral reduces to elementary functions. Thus, for

$$X=\frac{1+\beta R_1-\beta R_2}{2}$$

$$\beta^2R^2=\frac{(\beta^2R_1^2+\beta^2R_2^2)(1+\beta R_1+\beta R_2)^2-8\beta^4R_1^2R_2^2}{2[(1+\beta R_1+\beta R_2)^2-2(\beta^2R_1^2+\beta^2R_2^2)]} \tag{29}$$

Equation (28) may be solved by numerical-graphical methods. By a change of variable of the form

$$\xi=\frac{1+\beta R_1-\beta R_2}{2}+\frac{1+\beta R_1+\beta R_2}{2}\cos\theta$$

equation (28) is converted into the following form suitable for numerical integration:

$$\beta^2(R^2-R_2^2)=\frac{4\beta^2(R_1^2-R_2^2)(1+\beta R_1+\beta R_2)}{\pi(1-\beta R_1+\beta R_2)(1+3\beta R_1+\beta R_2)}\int_\pi^{\cos^{-1}\left[\frac{2(X-\beta R)-(1+\beta R_1-\beta R_2)}{1+\beta R_1+\beta R_2}\right]}\cos\theta\sqrt{\left(X-\frac{1+\beta R_1-\beta R_2}{2}-\frac{1+\beta R_1+\beta R_2}{2}\cos\theta\right)^2-\beta^2R^2}\,d\theta \tag{30}$$

The slope of the transition section at the general point (X, R) is found by differentiating equation (28). The result is

$$\frac{d(\beta R)}{dX}=\frac{\beta C}{RU}\int_{-\beta R_2}^{X-\beta R}\frac{\left(\frac{1+\beta R_1-\beta R_2}{2}-\xi\right)(X-\xi)d\xi}{\sqrt{(\xi+\beta R_2)(1+\beta R_1-\xi)}\sqrt{(X-\xi)^2-\beta^2R^2}}\left[1+\frac{\beta^2C}{U}\int_{-\beta R_2}^{X-\beta R}\frac{\left(\frac{1+\beta R_1-\beta R_2}{2}-\xi\right)d\xi}{\sqrt{(\xi+\beta R_2)(1+\beta R_1-\xi)}\sqrt{(X-\xi)^2-\beta^2R^2}}\right]^{-1} \tag{31}$$

For the general point, equation (31) is not integrable in elementary form. However, at the downstream end of the section ($X=1$, $R=R_1$) it may be integrated directly. The result is

$$\left[\frac{d(\beta R)}{dX}\right]_{\substack{X=1\\R=R_1}}=\left[\frac{\sqrt{\beta R_1}\,(1+\beta R_1-\beta R_2)(1+\beta R_1+3\beta R_2)}{\sqrt{2}\,(\beta^2R_1^2-\beta^2R_2^2)\sqrt{1+\beta R_1+\beta R_2}}-1\right]^{-1} \tag{32}$$

At the upstream end of the section, equation (31) may be evaluated by a suitable limiting process. For example, if $R=R_2$ and $X=\epsilon$ (where ϵ is a small quantity), the integrals in equation (31) may be evaluated if ϵ is neglected in comparison with quantities of the order of unity. After the evaluation, ϵ is allowed to vanish, and the result is

$$\left[\frac{d(\beta R)}{dX}\right]_{\substack{X=0\\R=R_2}}=\left[1+\frac{\sqrt{\beta R_2}\,(1-\beta R_1+\beta R_2)(1+3\beta R_1+\beta R_2)}{\sqrt{2}\sqrt{1+\beta R_1+\beta R_2}\,(\beta^2R_1^2-\beta^2R_2^2)}\right]^{-1} \tag{33}$$

For $R_2=0$ (the projectile tip), the front slope is equal to the slope of the Mach cone. The back slope is different from zero for $R_1\neq R_2$.

MINIMUM WAVE DRAG

The expression for the minimum wave drag is obtained by inserting the source-distribution function (eq. (26)) into the drag integral (eq. (16)). The expression for the drag of the transition section is

$$D=\frac{2\pi\rho U^2(R_1^2-R_2^2)^2}{(1-\beta R_1+\beta R_2)(1+3\beta R_1+\beta R_2)} \tag{34}$$

and the drag coefficient (based on the area of the section projected on a plane normal to its axis) is

$$C_D=\frac{4|R_1^2-R_2^2|}{(1-\beta R_1+\beta R_2)(1+3\beta R_1+\beta R_2)} \tag{35}$$

REVERSIBILITY

The results for the reverse-flow case may be obtained formally from the preceding direct-flow case by interchanging R_1 and R_2. If, in addition, X is replaced by $1-X$, the X-station will be measured from the same end of the configuration. The transition-section-shape expression (eq. (28)) can be shown to be an invariant relation between X and R under the transformation

$$R_1\rightarrow R_2$$

$$R_2\rightarrow R_1$$

$$X\rightarrow 1-X$$

Since the present analysis is a linear treatment, the reversibility of the minimum-drag shape cannot be considered as established to an order higher than the first.

The drag coefficient (eq. (35)) is not symmetrical in R_1 and R_2. However, β^2C_D is symmetrical to the first order in the small quantities βR_1 and βR_2 or, if βR_1 and βR_2 are not

small, $\beta^2 C_D$ is symmetrical to the first order in the quantities $\beta R_1 - \beta R_2$ and $\beta R_2 - \beta R_1$. The minimum wave drag thus is the same to the first order in the appropriate small quantities for the direct-flow and reverse-flow cases.

DISCUSSION OF RESULTS

The drag integral (eq. (12)) presented in this report depends upon the source-distribution function in the same way (except for slightly different weights of the kernel functions) that the slender-body drag expression (eq. (15)) depends upon the cross-sectional-area derivative. Since bodies with area-derivative discontinuities can be generated by continuous source distributions, equation (12) gives finite drag for certain types of bodies (for example, bodies with shoulders forward of the base) for which the usual slender-body drag expression diverges. The drag integral presented herein is thus applicable to a larger class of bodies than the Ward drag expression.

Some indication of the range of validity of equation (12) is given by a comparison of the values of drag calculated by various methods for several cones. Figures 3 (a), 3 (b), and 3 (c) present cone drag coefficients plotted against βR_1 for semivertex cones of 5°, 10°, and 15°, respectively. The drags are calculated by the following methods:

Method A—The drag integral (eq. (12)) with mass-flow continuity (eq. (17) with $R_2=0$) used as the boundary condition. Since the continuity condition is used in deriving the drag integral, this method uses a consistent boundary condition.

Method B—The solution of the linearized supersonic-flow equation for a cone ($f'(\xi)$=Constant) used with the exact boundary condition $\left(\frac{dr}{dx}=\frac{v_r}{U+v_x}\right)$ and the exact pressure equation. This method may be called the exact linear method. Van Dyke (ref. 12) has presented cone drags by this method.

Method C—The exact characteristics method for conical flow as given by reference 13.

Method D—The drag integral (eq. (12)) with the boundary condition $\frac{dr}{dx}=\frac{v_r}{U+v_x}$. This method was used only for the 5° cone. Each of the figures also shows the drag of the minimum-drag projectile tip of the same thickness ratio as was determined in the present analysis (curve I in fig. 3).

Figures 3 (a), 3 (b), and 3 (c) show that the drag integral with the continuity boundary condition (method A) gives cone drags closer to the exact value (method C) than the exact linear method (method B) for values of βR_1 less than approximately 0.30. From a comparison of methods A and D for the 5° cone, the divergence of the cone drag calculated by method A as $\beta R_1 \to 1.0$ is seen to be caused by the use of the mass-flow continuity boundary condition. These results indicate that equation (12) with equation (17) as the boundary condition gives good first-order results for Mach numbers above the transonic range and less than the Mach number at which the tangent of the Mach angle is less than approximately three times the slope of the body, that is, a moderate supersonic range.

Projectile tip ($R_2=0$).—Figure 4 presents two families of minimum-drag projectile-tip shapes ($\beta R_1=0.2$ and 0.4) calculated by equation (30). The Von Kármán projectile

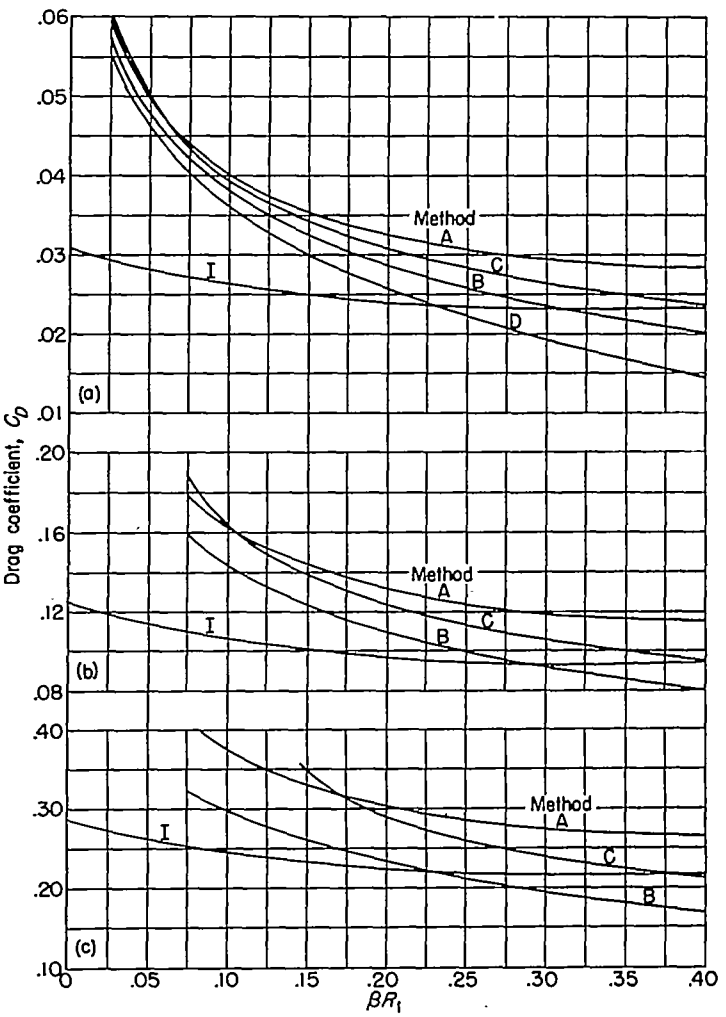

Method A	Drag integral with mass-flow-continuity boundary condition
Method B	Exact linear method
Method C	Exact characteristics method from reference 13
Method D	Drag integral with $\frac{dr}{dx}=\frac{v_r}{U-v_x}$
I	Drag coefficient of minimum-drag projectile tip

(a) 5° cone.
(b) 10° cone.
(c) 15° cone.

FIGURE 3.—Comparison of drag coefficients for three cones determined by several methods and for minimum-drag projectile tip of same thickness ratio as the cone.

tip and the limiting case $\beta R_1=1.0$ are shown for comparison. The Mach number and thickness-ratio dependence are related by the fact that the minimum-drag shape obeys the Göthert similarity rule (ref. 11). The slope at the base varies from zero to the cone slope as βR_1 varies from 0 to 1.0.

In both the Von Kármán analysis and the present analysis the basic assumptions of linearized theory are strongly violated at the nose of the projectile tip. Specific results of either analysis at the nose therefore cannot be accepted with confidence. However, inasmuch as linear theory often qualitatively predicts correct trends even outside its range of quantitative validity, it is interesting to note that in both analyses the nose of the minimum-drag projectile tip is as blunt as the analysis will allow (infinite slope for the Von Kármán tip and tangent to the Mach cone in the present analysis). It is probably true that the exact shape of a projectile tip for minimum wave drag has a blunt nose.

Figure 5 presents the ratio of the minimum-wave-drag coefficient based on the base area to the Von Kármán drag coefficient as a function of βR_1. The ratio has a minimum value at $\beta R_1=0.33$ and diverges as $\beta R_1\to 1.0$. The results

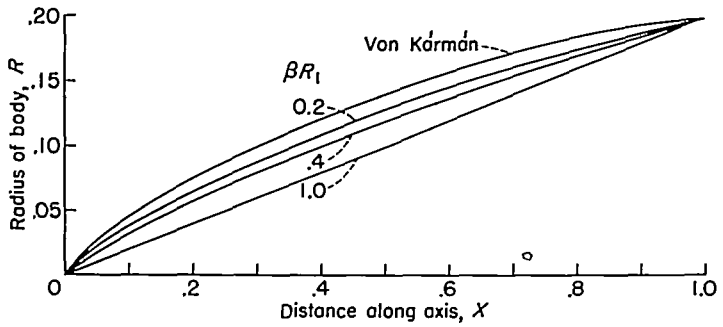

FIGURE 4.—Minimum-drag projectile-tip shapes. Von Kármán projectile tip is shown for comparison.

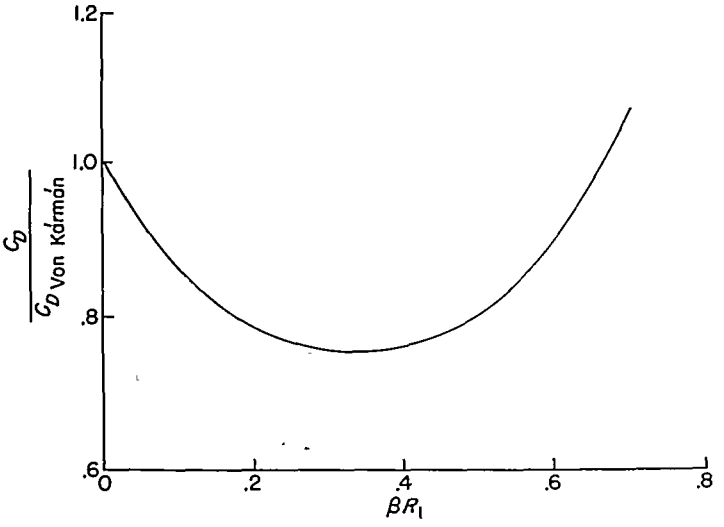

Figure 5.—Ratio of minimum-wave-drag coefficient to Von Kármán drag coefficient as a function of βR_1.

for the cone discussed previously suggest that the drag diverges as $\beta R_1\to 1.0$ because of the use of mass-flow continuity (eq. (17)) for the boundary condition and that the results are reasonably good for βR_1 less than about 0.3.

General case.—Figure 6 presents the radius at an intermediate point and the slopes at the two ends of the minimum-external-wave-drag transition section for four configurations with $\beta R_1-\beta R_2=0.4$. Figure 7 presents these three quantities for five configurations for which $\beta R_1-\beta R_2=0.05$. Equations (29), (32), and (33) indicate that for $\beta R_1-\beta R_2<\frac{1}{3}$ and $\beta R_1+\beta R_2>\dfrac{(\beta R_1-\beta R_2)(1+\beta R_1-\beta R_2)}{1-3(\beta R_1-\beta R_2)}$ the shape is a reverse curve lying within the truncated cone connecting the two cylinders for a distance downstream of the nose which increases as $\beta R_1-\beta R_2$ decreases. The entire shape was calculated by equation (30) for the case $\beta R_1-\beta R_2=0.05$ and $\beta R_1+\beta R_2=0.118$, which corresponds to the minimum front slope for $\beta R_1-\beta R_2=0.05$ (shown in fig. 7). This reverse-curve effect is more pronounced in the range of small values of $\beta R_1-\beta R_2$, the range where the linearized treatment is certainly correct.

For a comparison with the general case, the drag of a truncated-cone section for $\beta R_1-\beta R_2=0.05$, $\beta R_1+\beta R_2=0.118$, and $\beta=1$ was calculated by the method of reference 14. The truncated-cone drag coefficient (0.0228) is 18 percent higher than the minimum drag coefficient (0.0193).

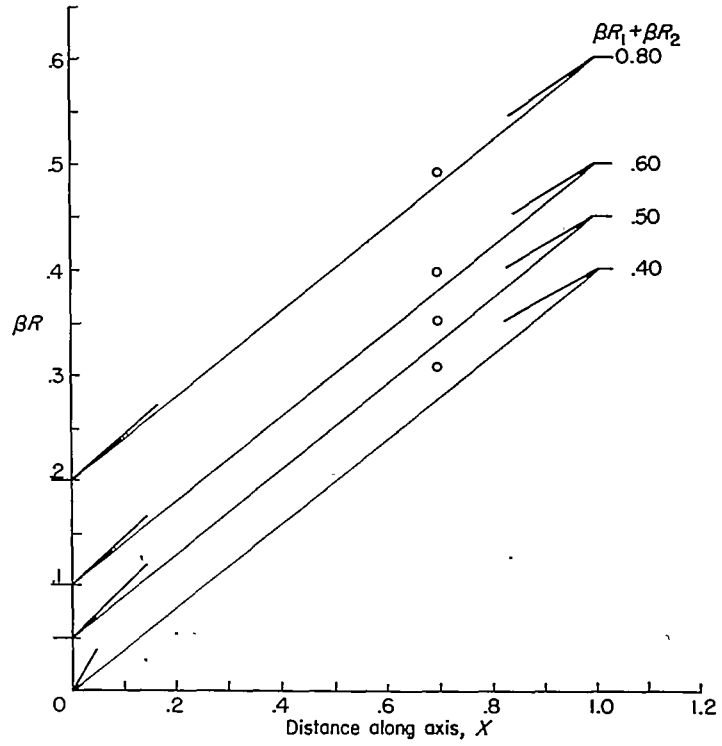

FIGURE 6.—Radius at intermediate point and slopes at two ends of minimum-external-drag transition section for four configurations. $\beta R_1-\beta R_2=0.4$.

CONCLUDING REMARKS

The drag integral for bodies of revolution at supersonic speeds is presented in a double-integral form depending explicitly upon the source-distribution function. The drag integral is applicable to a larger class of bodies than the usual slender-body drag expression and reduces to the Ward drag expression in the proper limit. Results for cones indicate that the drag integral with mass-flow continuity as the boundary condition gives good first-order results in the moderate supersonic range.

The minimum-wave-drag problem for a transition section connecting two semi-infinite cylinders is solved with the aid of a suitably chosen auxiliary condition. The source distribution, the minimum drag, the slopes at the two ends of the section, and the radius at an intermediate point are obtained in terms of elementary functions. The entire shape is obtained in an integral form amenable to numerical evaluation. The minimum-drag shape obeys the Göthert similarity rule. The minimum-drag shape and the minimum drag are unchanged to the first order when the flow direction is reversed. The projectile tip is a special case and is compared with the Von Kármán projectile tip.

LANGLEY AERONAUTICAL LABORATORY,
NATIONAL ADVISORY COMMITTEE FOR AERONAUTICS,
LANGLEY FIELD, VA., *March 1, 1954.*

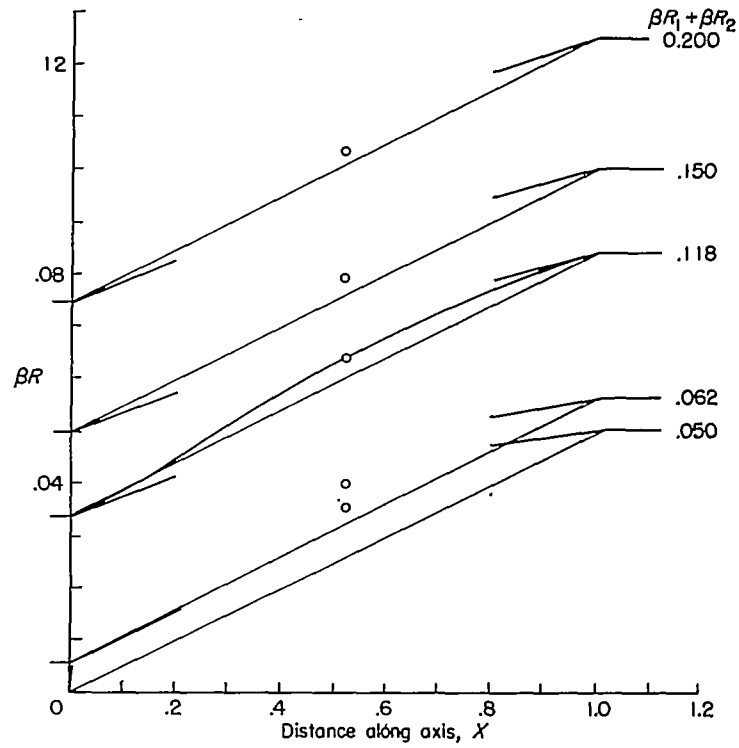

FIGURE 7.—Radius at intermediate point and slopes at two ends of minimum-external-drag transition section for five configurations. $\beta R_1-\beta R_2=0.05$. Entire contour shown for $\beta R_1+\beta R_2=0.118$.

APPENDIX

INTEGRATION IN EQUATION (11)

The integral of equation (11) is

$$I=\int_{\substack{\xi+\beta R_1\\ \eta+\beta R_1}}^{L}\frac{(x-\xi+x-\eta)\,dx}{\sqrt{(x-\xi)^2-\beta^2R_1^2}\sqrt{(x-\eta)^2-\beta^2R_1^2}} \tag{A1}$$

where the lower limit is the larger of the two quantities $\xi+\beta R_1$ or $\eta+\beta R_1$. The equation may be evaluated in the following manner. In order to convert the radicand in the denominator of the integrand into a quadratic function of the square of the integration variable, the variable is changed by using

$$x=S+\frac{\xi+\eta}{2} \tag{A2}$$

Substitution of equation (A2) into equation (A1) gives

$$I=\int_{S_0}^{S_L}\frac{2S\,dS}{\sqrt{S^4-2\left[\left(\frac{\xi-\eta}{2}\right)^2+\beta^2R_1^2\right]S^2+\left[\left(\frac{\xi-\eta}{2}\right)^2-\beta^2R_1^2\right]^2}} \tag{A3}$$

where S_L and S_0 are the appropriate limits for the variable S. Since the numerator of the integrand in equation (A3) is an odd polynomial in S, considerable simplification is effected by taking a new variable z proportional to S^2, such that

$$S^2=z+\left(\frac{\xi-\eta}{2}\right)^2+\beta^2R_1^2 \tag{A4}$$

Substituting equation (A4) into equation (A3) yields

$$I=\int_{z_0}^{z_L}\frac{dz}{\sqrt{z^2-\beta^2R_1^2(\xi-\eta)^2}}=\left[\cosh^{-1}\left|\frac{z}{\beta R_1(\xi-\eta)}\right|\right]_{z_0}^{z_L} \tag{A5}$$

or

$$I=\left[\cosh^{-1}\left|\frac{(x-\xi)(x-\eta)-\beta^2R_1^2}{\beta R_1(\xi-\eta)}\right|\right]_{\substack{\xi+\beta R_1\\ \eta+\beta R_1}}^{L}$$

$$=\cosh^{-1}\left|\frac{(L-\xi)(L-\eta)-\beta^2R_1^2}{\beta R_1(\xi-\eta)}\right| \tag{A6}$$

REFERENCES

1. Lighthill, M. J.: Supersonic Flow Past Bodies of Revolution. R. & M. No. 2003, British A.R.C., 1945.
2. Ward, G. N.: Supersonic Flow Past Slender Pointed Bodies. Quarterly Jour. Mech. and Appl. Math., vol. II, pt. 1, Mar. 1949, pp. 75–97.
3. Lighthill, M. J.: Supersonic Flow Past Slender Bodies of Revolution the Slope of Whose Meridian Section is Discontinuous Quarterly Jour. Mech. and Appl. Math., vol. I, pt. 1, Mar. 1948. pp. 90–102.
4. Von Kármán, Th.: The Problem of Resistance in Compressible Fluids. R. Accad. d'Italia, Cl. Sci. Fis., Mat. e Nat., vol. XIV, 1936 (Fifth Volta Congress held in Rome, Sept. 30–Oct. 6, 1935.)
5. Sears, William R.: On Projectiles of Minimum Wave Drag. Quarterly Appl. Math., vol. IV, no. 4, Jan. 1947, pp. 361–366.
6. Haack, W.: Projectile Shapes for Smallest Wave Drag. Translation No. A9–T–3, Contract W33–038–ac–15004(16351), ATI No. 27736, Air Materiel Command, U. S. Air Force, Brown Univ., 1948.
7. Busemann, A.: Heutiger Stand der Geschosstheorie. Bericht 139 der Lilienthal-Gesellschaft für Luftfahrtforschung, 1941, pp. 5–13.
8. Ferrari, Carlo: The Body and Ogival Contour Giving Minimum Wave Drag. Rep. No. CAL–55, Cornell Aero. Lab., Inc., Oct. 1951.
9. Ferrari, Carlo: Determination of the External Contour of a Body of Revolution With a Central Duct So As To Give Minimum Drag in Supersonic Flow, With Various Perimetral Conditions Imposed Upon the Missile Geometry. Rep. No. AF–814–A–1 (Contract No. N6ori–119, T. O. IV), Cornell Aero. Lab., Inc., Mar. 1953.
10. Lamb, Horace: Hydrodynamics. Sixth ed., Cambridge Univ. Press, 1932, p. 527.
11. Göthert, B.: Plane and Three-Dimensional Flow at High Subsonic Speeds. NACA TM 1105, 1946.
12. Van Dyke, Milton D.: A Study of Second-Order Supersonic Flow Theory. NACA Rep. 1081, 1952. (Supersedes NACA TN 2200.)
13. Staff of the Computing Section, Center of Analysis (Under Direction of Zdeněk Kopal): Tables of Supersonic Flow Around Cones. Tech. Rep. No. 1, M. I. T., 1947.
14. Brown, Clinton E., and Parker, Hermon M.: A Method for the Calculation of External Lift, Moment, and Pressure Drag of Slender Open-Nose Bodies of Revolution at Supersonic Speeds. NACA Rep. 808, 1945. (Supersedes NACA WR L–720.)

413672—57——9